Distributed Coordinated Control for Fixed-Wing UAVs with Dynamic Event-Triggered Communication

Zhang, Boyang; Sun, Xiuxia; Lv, Maolong; Liu, Shuguang

Citation (APA)
Zhang, B., Sun, X., Lv, M., & Liu, S. (2022). Distributed Coordinated Control for Fixed-Wing UAVs with Dynamic Event-Triggered Communication. *IEEE Transactions on Vehicular Technology*, *71*(5), 4665-4676. https://doi.org/10.1109/TVT.2022.3140771

Important note
To cite this publication, please use the final published version (if applicable).
Please check the document version above.

Distributed Coordinated Control for Fixed-Wing UAVs With Dynamic Event-Triggered Communication

Boyang Zhang , Xiuxia Sun, Maolong Lv , and Shuguang Liu

Abstract—Compared with most existing results concerning unmanned aerial vehicles (UAVs) wherein two-degree or only attitude/longitudinal dynamics are considered, this paper proposes an event-based fault-tolerant coordinated control (FTC) for multiple fixed-wing UAVs such that the consensus tracking of velocity and attitude is achieved in the presence of actuator faults, external disturbances and modeling uncertainties. More precisely, as opposed to static event-triggered communication mechanisms, a dynamic event-triggered communication mechanism (DECM) is devised to schedule the connected communications while avoiding the unnecessary information exchanges among UAVs, which reduces the communication burden and saves on the network resources. Meanwhile, the Zeno phenomenon is excluded in terms of guaranteeing that the period between two consecutive triggering communication is lower bounded by a positive constant. Moreover, the actuator fault, external disturbance as well as model uncertainty are treated as the lumped disturbances and estimated via the disturbance observer technique. By strict Lyapunov arguments, all closed-loop signals are proved to be uniformly ultimately bounded (UUB) and the tracking errors of velocity and attitude converge to a residual set around origin. Finally, simulation results are presented to illustrate the validity and superiority of proposed event-based control scheme.

Index Terms—Dynamic event-triggered communication mechanism, fault-tolerant control, fixed-wing unmanned aerial vehicles.

NOMENCLATURE

ϕ_i	Roll angle
ϕ_r	Reference command of ϕ_i
ψ_i	Yaw angle
ψ_r	Reference command of ψ_i
ρ	Air density
θ_i	Pitch angle
θ_r	Reference command of θ_i
m_i	Vehicle mass
p_i	Angular velocity in X of body fixed frame
q_i	Angular velocity in Y of body fixed frame
r_i	Angular velocity in Z of body fixed frame
u_i	Linear velocity in X of body fixed frame
V_i	Total speed in body fixed frame
v_i	Linear velocity in Y of body fixed frame
V_r	Reference command of V_i
w_i	Linear velocity in Z of body fixed frame
α_i	Attack angle
$\bar{c}_i$	Mean aerodynamic chord
$\bar{q}_i$	Dynamic pressure
β_i	Sideslip angle
$\boldsymbol{\delta}_i$	Flight control surface
$\boldsymbol{S}(\bullet)$	Skew-symmetric matrix
δ_{ai}	Aileron angular deflection
δ_{ei}	Elevator angular deflection
δ_{ri}	Rudder angular deflection
$\lambda_{\max}(\bullet)$	Maximum eigenvalues of a matrix
$\lambda_{\min}(\bullet)$	Minimum eigenvalues of a matrix
$\Re^m$	Real m-vector
$\Re^{m \times n}$	Real $m \times n$ matric
$\mathrm{SO}(3)$	Third-order Special Orthogonal group
b_i	Wingspan
S_i	Wing surface area
$\boldsymbol{\omega}_i$	Non-inertial expression of angular velocity
$\boldsymbol{\varphi}_i$	Attitude described by Euler angles
$\boldsymbol{\varphi}_r$	Reference command of $\boldsymbol{\varphi}_i$
$\boldsymbol{d}_{\omega i}$	External disturbances in angular velocity
$\boldsymbol{d}_{vi}$	External disturbances in velocity
$\boldsymbol{F}_i$	Aerodynamics force
$\boldsymbol{g}$	Gravity acceleration
$\boldsymbol{J}_i$	Inertia tensor
$\boldsymbol{N}_i$	Aerodynamics moment
$\boldsymbol{p}_i$	Inertial position
$\boldsymbol{T}_i$	Thrust vector along x body axis
$\boldsymbol{v}_i$	Non-inertial expression of linear velocity
$\| \cdot \|$	Euclidean norm of a vector

I. INTRODUCTION

COORDINATED flight of multiple fixed-wing unmanned aerial vehicles (UAVs) has been extensively studied over the past decades, due to its important role in achieving flexibility and cost effectiveness of mission cooperation [1]–[3]. Generally,

coordinated control problem has been investigated in several aspects, including formulating and maintaining a particular formation shape for UAVs in a group [4], and synchronous tracking of velocity and attitude for UAV formation [5]. In particular, distributed control for coordination part is now in research spotlight thanks to its undeniable benefits that global information is no longer required in control design, while preserving closed-loop stability [6], [7]. Driven by the distributed coordinated control, various advanced results for multiple UAVs are currently available in [8]–[11] (just to name a few). Typically, [8] investigated the attitude synchronization tracking problem of networked UAVs in a distributed cooperative control framework. [9] explored the distributed cooperative fault-tolerant control for longitudinal synchronization tracking of multiple UAVs with actuator faults and input saturation. Further, in [10], a distributed model predictive approach with swarm intelligence was designed for the coordinated control of multiple UAVs. In [11], a distributed vector-field based control scheme was proposed to achieve the path following and circular motion around the target for UAV formation.

However, all aforementioned methods [8]–[11] are performed based on the simplified two-degree models [10], [11], or just taking the attitude/longitudinal dynamics into consideration [8], [9]. Such the model simplification unavoidably lowers the system description precision, and thus cannot accurately describe the practical UAV system. Actually, the fixed-wing UAV system is a typical nonlinear model with decomposed translational and rotational dynamics. Therefore, designing the velocity and attitude control for translational and rotational dynamics is an open and important problem.

Moreover, note that existing literatures [8]–[14] focus on the coordinated control problem of UAVs subject to continuous-time information exchange regardless of the consumption of network resources such as bandwidth and energy. Especially for the co-operative UAV flight, this drawback will become more apparent as the number of UAVs increases. Therefore, in order to mitigate the unnecessary information exchanges and reduce the channel load, an energy-efficient option namely event-triggered communication strategy [15] has been developed, which schedules the inter-agent communication when the triggering condition is satisfied.

Different from the traditional periodic communication, the event-triggered communication relies on a state-dependent triggering condition. Based on the event-triggered communication mechanism, distributed tracking control protocols are designed for single-integrator agents [16], second-order agents [17], linear agents [18] and nonlinear multi-agent systems [19], [20]. Although effective performances with event-triggered communications are obtained in [16]–[20], it can be noted that these triggering functions are with fixed threshold values. Nevertheless, for some complex dynamic situations, it is unreasonable to permanently fix the threshold parameter. In this case, the threshold value should dynamically change to reflect the real-time data transmission rates [21]. Therefore, the dynamic triggering rules are proposed and successfully applied in the linearized dynamics of multi-agent system [22], [23] and linear cases of individual system [24], [25]. However, it is noted that studies

of [22]–[25] just consider the linear dynamics of agent systems without regard to nonlinear dynamics, let alone the practical UAV system. Therefore, the crucial question of how to design a novel dynamic triggering mechanism for UAV systems still remains open. Moreover, since practical UAV system inevitably suffers from actuator faults, which would degrade the flight performance and even lead to instability, fault-tolerant control has become another significant research problem and some effective fault-tolerant control approaches for UAVs have been reported in [8], [9], [9]–[28].

Motivated by the foregoing analyses, the main contributions of this work are three-fold below:

- As opposed to the existing results [8]–[11] which are either concentrated on attitude/longitudinal motions or two-degree dynamics, this study proposes an event-based fault-tolerant coordinated control scheme for multi-UAVs such that the consensus tracking of velocity and attitude is achieved subject to actuator faults, external disturbances and modeling uncertainties.
- In contrast to the static event-triggered communication mechanisms [16]–[20], the proposed triggering function using state values is determined by a dynamic rule. It can achieve a better tradeoff between reducing communication burden and preserving favorable tracking performance. Meanwhile, the Zeno phenomenon is precluded to guarantee that the time between two consecutive communications is lower bounded by a positive constant.
- Unlike the existing cooperative flight of UAVs dependent on the periodic communication of neighbors' states [8]–[14], the proposed distributed control scheme merely utilizes locally triggered states of underlying neighbors at discretized event-based instants, thus significantly relaxing the pressure on the communication network.

The rest of paper is organized as follows. The multi-UAV dynamics, communication theory and control objective are presented in Section II. Section III gives the details of cooperative event-based control design. Section IV shows the simulation validations, and Section V draws the conclusions.

II. PROBLEM FORMULATION AND PRELIMINARIES

A. UAV Kinematics and Dynamics

Consider a team of N identical fixed-wing UAVs. For the ith UAV, the full dynamics is given by (see Fig. 1) [29]

$$\dot{\boldsymbol{p}}_i = \boldsymbol{R}_1\left(\boldsymbol{\varphi}_i\right)\boldsymbol{v}_i \tag{1}$$

$$\dot{\boldsymbol{v}}_i = -\boldsymbol{S}\left(\boldsymbol{\omega}_i\right)\boldsymbol{v}_i + \frac{\boldsymbol{T}_i}{m_i} + \boldsymbol{R}_1^{\mathrm{T}}\left(\boldsymbol{\varphi}_i\right)\boldsymbol{g} + \frac{\boldsymbol{F}_i}{m_i} + \boldsymbol{d}_{vi} \tag{2}$$

$$\dot{\boldsymbol{\varphi}}_i = \boldsymbol{R}_2^{-1}\left(\boldsymbol{\varphi}_i\right)\boldsymbol{\omega}_i \tag{3}$$

$$\boldsymbol{J}_i\dot{\boldsymbol{\omega}}_i = -\boldsymbol{\omega}_i \times \boldsymbol{J}_i\boldsymbol{\omega}_i + \boldsymbol{N}_i + \boldsymbol{C}\left(\boldsymbol{\delta}_i\right)\boldsymbol{\delta}_i + \boldsymbol{J}_i\boldsymbol{d}_{\omega i} \tag{4}$$

where $\boldsymbol{p}_i = [x_i, y_i, z_i]^{\mathrm{T}}$ denotes the inertial position, $\boldsymbol{v}_i = [u_i, v_i, w_i]^{\mathrm{T}}$ is the linear velocity, $\boldsymbol{\varphi}_i = [\phi_i, \theta_i, \psi_i]^{\mathrm{T}}$ represents the attitude angle, $\boldsymbol{\omega}_i = [p_i, q_i, r_i]^{\mathrm{T}}$ denotes the angular velocity. Moreover, $\boldsymbol{T}_i = [T_{xi}, 0, 0]^{\mathrm{T}}$ is the thrust vector along x body axis, $\boldsymbol{\delta}_i = [\delta_{ai}, \delta_{ei}, \delta_{ri}]^{\mathrm{T}}$ is the control input, where δ_{ai}, δ_{ei},
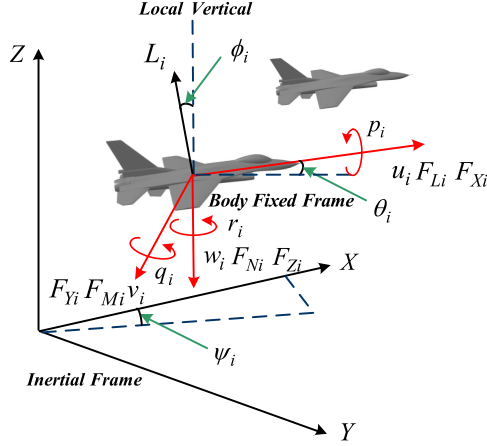
Fig. 1. Dynamical behavior of fixed-wing UAV model.

δ_{ri} represent the deflection of aileron, elevator and rudder respectively, m_i is the vehicle mass, $\boldsymbol{g} = [0, 0, g_z]^{\mathrm{T}}$ is the gravity acceleration in inertia frame, $\boldsymbol{d}_{vi} \in \Re^3$ and $\boldsymbol{d}_{\omega i} \in \Re^3$ are the unknown bounded external disturbances, $\boldsymbol{J}_i$ is the inertia tensor with the symmetric $x - z$ plane

$$\boldsymbol{J}_i = \begin{bmatrix} J_{xi} & 0 & -J_{xzi} \\ 0 & J_{yi} & 0 \\ -J_{zxi} & 0 & J_{zi} \end{bmatrix} \quad (5)$$

Besides, $\boldsymbol{R}_1(\boldsymbol{\varphi}_i) \in \mathrm{SO}(3)$ is the rotation matrix transforming the body frame coordinates to inertial axis coordinates, and the matrix $\boldsymbol{R}_2(\boldsymbol{\varphi}_i) \in \Re^{3 \times 3}$ maps the time derivative of attitude angles to the non-inertial expression of angular velocity.

$$\boldsymbol{R}_1(\boldsymbol{\varphi}_i) = \begin{bmatrix} c_{\psi_i} c_{\theta_i} & -s_{\psi_i} s_{\phi_i} + c_{\psi_i} s_{\theta_i} s_{\phi_i} & s_{\psi_i} s_{\phi_i} + c_{\psi_i} s_{\theta_i} c_{\phi_i} \\ s_{\psi_i} c_{\theta_i} & c_{\psi_i} c_{\phi_i} + s_{\psi_i} s_{\theta_i} s_{\phi_i} & -c_{\psi_i} s_{\phi_i} + s_{\psi_i} s_{\theta_i} c_{\phi_i} \\ -s_{\theta_i} & c_{\theta_i} s_{\phi_i} & c_{\theta_i} c_{\phi_i} \end{bmatrix}$$

$$\boldsymbol{R}_2(\boldsymbol{\varphi}_i) = \begin{bmatrix} 1 & 0 & -s_{\psi_i} \\ 0 & c_{\psi_i} & s_{\psi_i} c_{\theta_i} \\ 0 & -s_{\theta_i} & c_{\psi_i} c_{\theta_i} \end{bmatrix} \quad (6)$$

where s_a and c_a stand for $\sin a$ and $\cos a$ functions respectively. The aerodynamics force $\boldsymbol{F}_i = [F_{Xi}, F_{Yi}, F_{Zi}]^{\mathrm{T}}$ and moment $\boldsymbol{N}_i = [F_{Li}, F_{Mi}, F_{Ni}]^{\mathrm{T}}$ are calculated in terms of aerodynamic coefficients.

$$\boldsymbol{F}_i = \bar{q}_i S_i \boldsymbol{R}_3^{-1}(\alpha_i, \beta_i)[-C_{Di}, C_{Yi}, -C_{Li}]^{\mathrm{T}} \quad (7)$$

$$\boldsymbol{N}_i = \bar{q}_i S_i [b_i C'_{li}, \bar{c}_i C'_{Mi}, b_i C'_{ni}]^{\mathrm{T}} \quad (8)$$

where $\alpha_i = \arctan(w_i/u_i)$ and $\beta_i = \arcsin(u_i/v_i)$ denote the attack angle and sideslip angle respectively. $\bar{q}_i = \frac{1}{2}\rho V_i^2$ is the dynamic pressure with total velocity $V_i = \sqrt{u_i^2 + v_i^2 + w_i^2}$. Air density ρ, wingspan b_i, wing surface area S_i and mean aerodynamic chord $\bar{c}_i$ are constants. The transformation matrix $\boldsymbol{R}_3(\alpha_i, \beta_i)$ is

$$\boldsymbol{R}_3(\alpha_i, \beta_i) = \begin{bmatrix} c_{\alpha_i} c_{\beta_i} & s_{\beta_i} & s_{\alpha_i} c_{\beta_i} \\ -c_{\alpha_i} s_{\beta_i} & c_{\beta_i} & -s_{\alpha_i} s_{\beta_i} \\ -s_{\alpha_i} & 0 & c_{\alpha_i} \end{bmatrix} \quad (9)$$

And $C_{Di}, C_{Yi}, C_{Li}, C'_{li}, C'_{Mi}$, and C'_{ni} are the dimensionless coefficients in force/moment expression, of which the detailed

descriptions are shown in [30]. The control effectiveness matrix $\boldsymbol{C}(\boldsymbol{\delta}_i)$ is presented as

$$\boldsymbol{C}(\boldsymbol{\delta}_i) = \begin{bmatrix} \bar{q}_i S_i b_i c_{l\delta_{ai}} & 0 & \bar{q}_i S_i b_i c_{l\delta_{ri}} \\ 0 & \bar{q}_i S_i \bar{c}_i c_{m\delta_{ei}} & 0 \\ \bar{q}_i S_i b_i c_{n\delta_{ai}} & 0 & \bar{q}_i S_i b_i c_{n\delta_{ri}} \end{bmatrix} \quad (10)$$

B. Control-Oriented Model With Actuator Faults and Modeling Uncertainties

Following the descriptions in [29], [30], the fixed-wing UAV system can be decomposed into two interconnected subsystems, i.e., translational dynamics (2) and rotational dynamics (3)–(4). This allows the translational and rotational dynamics to remain in their original forms. In line with [31], considering the time response of translation dynamics with regard to rotational dynamics, it is reasonable to deal with the rotational control problem and translational control problem separately, such that the rotational control action is to be executed, followed by the translational controller.

1) Translational Kinematics: From (2), taking the time derivative of velocity denotes

$$\dot{V}_i = \frac{\boldsymbol{v}_i^{\mathrm{T}} \dot{\boldsymbol{v}}_i}{V_i} = \frac{\boldsymbol{v}_i^{\mathrm{T}}}{V_i} \left(-\boldsymbol{S}(\boldsymbol{\omega}_i) \boldsymbol{v}_i + \frac{\boldsymbol{T}_i}{m_i} + \boldsymbol{R}_1^{\mathrm{T}}(\boldsymbol{\varphi}_i) \boldsymbol{g} + \frac{\boldsymbol{F}_i}{m_i} + \boldsymbol{d}_{vi} \right) \quad (11)$$

Based on (11), the thrust is extracted. With the property $\boldsymbol{v}_i^{\mathrm{T}} \boldsymbol{S}(\boldsymbol{\omega}_i) \boldsymbol{v}_i = 0$, it follows that

$$\dot{V}_i = \frac{u_i T_{xi}}{m_i V_i} + \frac{\boldsymbol{v}_i^{\mathrm{T}}}{V_i} \left(\boldsymbol{R}_1^{\mathrm{T}}(\boldsymbol{\varphi}_i) \boldsymbol{g} + \frac{\boldsymbol{F}_i}{m_i} + \boldsymbol{d}_{vi} \right) \quad (12)$$

Remark 1: Since the UAV model is clearly underactuated, T_{xi} simply acts on velocity component u_i, and there are no direct controls for velocity components w_i and v_i. Whereas with the relationship $w_i = u_i \tan \alpha_i$ and $v_i = u_i/\sin \beta_i$, it is still controllable to regulate the components w_i, v_i, that is to point $\boldsymbol{v}_i$ in a desired direction by adding additional controls on α_i and β_i.

During flight, the thrust possibly suffers from actuator faults, modeled by [29]

$$T_{xi} = \rho_{T_i} T_{xi0} + T_{xif}, \quad (13)$$

where T_{xi0} is the designed control input, ρ_{T_i} is the unknown actuator efficiency factor satisfying $0 \leq \rho_{T_i} \leq 1$ and T_{xif} is the bounded unknown bias fault. It follows along (13) that
1) $\rho_{T_i} = 1$ and $T_{xif} = 0$. This means the fault-free case.
2) $0 < \rho_{T_i} < 1$ and $T_{xif} = 0$. This indicates the partial loss of effectiveness.
3) $\rho_{T_i} = 1$ and $T_{xif} \neq 0$. This indicates the bias fault.
4) $\rho_{T_i} = 0$ and $T_{xif} \neq 0$. This means that T_{xi} is stuck at bounded time-varying function T_{xif}.

Besides, note that the accurate information of $\boldsymbol{F}_i$ cannot be known a priori due to the coefficient uncertainties. In this sense, $\boldsymbol{F}_i$ is decomposed into a known component $\boldsymbol{F}_{i0}$ and an uncertain one $\Delta \boldsymbol{F}_i$.

Then with actuator faults and modeling uncertainties, the dynamics of (12) is rewritten as

$$\dot{V}_i = \frac{u_i T_{xi0}}{m_i V_i} + \frac{\boldsymbol{v}_i^{\mathrm{T}}}{V_i}\left(\boldsymbol{R}_1^{\mathrm{T}}\left(\boldsymbol{\varphi}_i\right)\boldsymbol{g} + \frac{\boldsymbol{F}_{i0}}{m_i}\right) + \Delta_{vi} \quad (14)$$

where $\Delta_{vi} = \frac{(\rho_{Ti}-1)u_i T_{xi0}}{m_i V_i} + \frac{u_i T_{xif}}{m_i V_i} + \frac{\boldsymbol{v}_i^{\mathrm{T}}}{V_i}\left(\frac{\Delta \boldsymbol{F}_i}{m_i} + \boldsymbol{d}_{vi}\right)$ is the lumped disturbances induced by the actuator faults and modeling uncertainties.

2) Rotational Kinematics: From (4), considering the coefficient uncertainties, $\boldsymbol{\omega}_i \times \boldsymbol{J}_i \boldsymbol{\omega}_i$ is decomposed into a known component $\boldsymbol{\omega}_i \times \boldsymbol{J}_{i0} \boldsymbol{\omega}_i$ and an uncertain one $\boldsymbol{\omega}_i \times \Delta \boldsymbol{J}_i \boldsymbol{\omega}_i$. Similarly, $\boldsymbol{N}_i$ is composed by a known part $\boldsymbol{N}_{i0}$ and an uncertain one $\Delta \boldsymbol{N}_i$. Also, $\boldsymbol{C}(\boldsymbol{\delta}_i)$ consists of a known component $\boldsymbol{C}_0(\boldsymbol{\delta}_i)$ and an uncertain term $\Delta \boldsymbol{C}(\boldsymbol{\delta}_i)$.

Moreover, during flight the flight control surfaces inevitably suffer from actuator faults, given by [29]

$$\delta_{li} = \rho_{\delta_{li}}\delta_{li0} + \delta_{lif} \quad (15)$$

where δ_{li0} is the designed control input with $l = \{a, e, r\}$, $\rho_{\delta_{li}}$ is the unknown actuator efficiency factor satisfying $0 \leq \rho_{\delta_{li}} \leq 1$, and δ_{lif} is the bounded unknown bias fault. Based on (15), consider the following cases:

1) $\rho_{\delta_{li}} = 1$ and $\delta_{lif} = 0$. This refers to the fault-free case.
2) $0 < \rho_{\delta_{li}} < 1$ and $\delta_{lif} = 0$. This indicates the partial loss of effectiveness.
3) $\rho_{\delta_{li}} = 1$ and $\delta_{lif} \neq 0$. This means the bias fault.
4) $\rho_{\delta_{li}} = 1$ and $\delta_{lif} \neq 0$. This implies that δ_{li} is stuck at bounded time-varying function δ_{lif}.

Then, the actuator fault model (15) is reformulated as

$$\boldsymbol{\delta}_i = \boldsymbol{\rho}_{\delta_i}\boldsymbol{\delta}_{i0} + \boldsymbol{\delta}_{if}, \quad (16)$$

where $\boldsymbol{\delta}_{i0} = [\delta_{ai0}, \delta_{ei0}, \delta_{ri0}]^{\mathrm{T}}$, $\boldsymbol{\rho}_{\delta_i} = \mathrm{diag}\{\rho_{\delta_{ai}}, \rho_{\delta_{ei}}, \rho_{\delta_{ri}}\}$, $\boldsymbol{\delta}_{if} = [\delta_{aif}, \delta_{eif}, \delta_{rif}]^{\mathrm{T}}$.

Considering above actuator faults and modeling uncertainties, the angular velocity model (4) is rewritten as

$$\boldsymbol{J}_{i0}\dot{\boldsymbol{\omega}}_i = -\boldsymbol{\omega}_i \times \boldsymbol{J}_{i0}\boldsymbol{\omega}_i + \boldsymbol{N}_{i0} + \boldsymbol{C}_{i0}\boldsymbol{\delta}_{i0} + \boldsymbol{\Delta}_{\omega i} \quad (17)$$

where $\boldsymbol{\Delta}_{\omega i} = -\Delta \boldsymbol{J}_i \dot{\boldsymbol{\omega}}_i - \boldsymbol{\omega}_i \times \Delta \boldsymbol{J}_i \boldsymbol{\omega}_i + \Delta \boldsymbol{N}_i + \boldsymbol{C}_{i0}\boldsymbol{\delta}_{if} + \boldsymbol{C}_{i0}(\boldsymbol{\rho}_i - \boldsymbol{I}_3)\boldsymbol{\delta}_{i0} + \Delta \boldsymbol{C}_i \boldsymbol{\delta}_i + \boldsymbol{J}_i \boldsymbol{d}_{\omega i}$ is the lumped uncertainties induced by the actuator faults and modeling uncertainties.

Remark 2: In [8], only the attitude model (rotational dynamics) is studied. While in [9], the longitudinal dynamics is just considered. Meanwhile, [10], [11] regard each UAV as a mass point, neglecting the problem of body posture. In the perspective of fixed-wing UAV, our paper focus on the underlying control of both translational and rotational dynamics. With the control law stabilizing the rotational dynamics through δ_{ai}, δ_{ei} and δ_{ri}, the translational dynamics are controlled by T_{xi}.

C. Graph Theory

The undirected graph always describes the connections among the multiple UAVs. Given an undirected graph $\mathcal{G} = (\mathcal{V}, \mathcal{E}, \mathcal{A})$, it consists of nodes $\mathcal{V} = \{v_1, \ldots, v_n\}$ and the sets of edges $\mathcal{E} = \{(i, j), i, j \in \mathcal{V}, \text{and } i \neq j\}$, and $\mathcal{A} = [a_{ij}] \in \Re^{n \times n}$ denotes the weighted adjacency matrix of $\mathcal{G}$. If there exists an edge between node i and j, then $a_{ij} = a_{ji} \neq 0$ and otherwise

$a_{ij} = a_{ji} = 0$. Moreover, a_{ii} equals to 0 for all $i \in \mathcal{V}$. The neighbors of node i is denoted by the set $\mathcal{N}_i = \{v_j : (v_j, v_i) \in \mathcal{E}\}$. The Laplacian matrix is defined by $\mathcal{L} = \mathcal{D} - \mathcal{A}$, where $\mathcal{D} = \mathrm{diag}\{d_1, \ldots, d_n\}$ with $d_i = \sum_{j=1}^{n} a_{ij}$. $\mathcal{G}$ is connected if there is a path from every node to each other node. Moreover, consider the virtual leader governed by same dynamics as (1)–(4), where V_r, $\boldsymbol{\varphi}_r$ are velocity and attitude angles of the virtual leader, respectively.

For analysis, some useful lemmas and assumptions are made as follows:

Lemma 1 ([32]): The Laplacian matrix $\mathcal{L}$ is symmetric positive semidefinite under the assumption that $\mathcal{G}$ is an undirected graph.

Lemma 2 ([33]): For $\boldsymbol{x}_i \in \Re^m$, $\boldsymbol{y}_i \in \Re^m$, $\boldsymbol{y}_j \in \Re^m$, $\boldsymbol{K}_i \in \Re^{m \times m}$ and $\mathcal{A} = [a_{ij}] \in \Re^{n \times n}$, if $\mathcal{A}$ is symmetric, it holds that

$$\sum_{i=1}^{n}\sum_{j=1}^{n} a_{ij}\boldsymbol{x}_i^{\mathrm{T}}\tanh\left(\boldsymbol{K}_i\left(\boldsymbol{y}_i - \boldsymbol{y}_j\right)\right)$$

$$= \frac{1}{2}\sum_{i=1}^{n}\sum_{j=1}^{n} a_{ij}(\boldsymbol{x}_i - \boldsymbol{x}_j)^{\mathrm{T}}\tanh\left(\boldsymbol{K}_i\left(\boldsymbol{y}_i - \boldsymbol{y}_j\right)\right) \quad (18)$$

Lemma 3 ([34]): Given $\boldsymbol{x}_i \in \Re^n$, the following inequation holds:

$$\boldsymbol{x}_i^{\mathrm{T}}\tanh\left(\boldsymbol{x}_i\right) \geq \tanh^{\mathrm{T}}\left(\boldsymbol{x}_i\right)\tanh\left(\boldsymbol{x}_i\right) \geq 0 \quad (19)$$

Assumption 1: The graph $\mathcal{G}$ is undirected and connected and V_r, $\boldsymbol{\varphi}_r$ are directly available to all UAVs.

D. Control Objective

Consider a group of N UAVs with event-triggered communication graph. The aim is to design the distributed cooperative tracking controller with dynamic event-triggered communication mechanism such that

- All the closed-loop signals are uniformly ultimately bounded (UUB).
- The leader-following consensus tracking for velocity and attitude is guaranteed by $\lim_{t \to \infty}|V_i - V_r| = 0$, $\lim_{t \to \infty}\|\boldsymbol{\varphi}_i - \boldsymbol{\varphi}_r\| = 0$, $i = 1, 2, \ldots N$, in the presence of actuator faults, external disturbances and model uncertainties.
- The communication burden for multi-UAV system is considerably reduced. Meantime, the Zeno behavior is precluded such that the time between two consecutive broadcasts is lower bounded by a positive constant.

III. EVENT-BASED COORDINATED CONTROLLER DESIGN

A. Dynamic Event-Triggered Communication Mechanism

We are at the position to provide the triggering communication conditions for translational and rotational kinematics, respectively.

1) Translational Kinematics: Define $\tilde{V}_i = V_i - V_r$. The triggering function for velocity tracking is presented as

$$f_i\left(t, e_{vi}(t)\right) = |e_{vi}(t)| - \varsigma_{v2}$$

$$-\frac{\alpha_v \sum_{j\in\mathcal{N}_i} a_{ij}\left|\tanh\left(\tilde{V}_i\left(t_{k_i}^{vi}\right) - \tilde{V}_j\left(t_{k_j}^{vj}\right)\right)\right|^2}{2\left(\left|\sum_{j\in\mathcal{N}_i} a_{ij}\tanh\left(\tilde{V}_i\left(t_{k_i}^{vi}\right) - \tilde{V}_j\left(t_{k_j}^{vj}\right)\right)\right| + \varsigma_{v1}\right)} \quad (20)$$

where $0 < \alpha_v < 1$, $\varsigma_{v1} > 0$, $\varsigma_{v2} = e^{c_{v1}\tanh(c_{v2}t)}$ is a turning function with $c_{v1} > 0$, $c_{v2} > 0$, $t_{k_i}^{vi}$ ($k_i = 1, 2, \ldots$) is the latest triggering instant of velocity channel, $e_{vi}(t)$ is the state-based error between the sampled state and continuous state, defined as $e_{vi}(t) = \tilde{V}_i(t_{k_i}^{vi}) - \tilde{V}_i(t)$, $t \in [t_{k_i}^{vi}, t_{k_i+1}^{vi})$, where $t_{k_i+1}^{vi} := \inf\{t > t_{k_i}^{vi} + \tau_{\min}^{vi} | f_i(t, e_{vi}(t)) > 0\}$ with $\tau_{\min}^{vi} \in \Re_{>0}$ being the minimum inter-event time of velocity tracking.

2) Rotational Kinematics: Define $\check{\varphi}_i = \varphi_i - \varphi_r$, $\tilde{\omega}_i = \omega_i - \omega_{di}$, where ω_{di} is the designed intermediate control. Then the triggering function for attitude tracking gives

$$f_i(t, \boldsymbol{e}_{\varphi i}(t)) = \|\boldsymbol{e}_{\varphi i}(t)\| - \varsigma_{\varphi 2}$$
$$-\frac{\alpha_\varphi \sum_{j\in\mathcal{N}_i} a_{ij}\left\|\tanh\left(\tilde{\boldsymbol{\omega}}_i\left(t_{k_i}^{\varphi i}\right) - \tilde{\boldsymbol{\omega}}_j\left(t_{k_j}^{\varphi j}\right)\right)\right\|^2}{2\left(\left\|\sum_{j\in\mathcal{N}_i} a_{ij}\tanh\left(\tilde{\boldsymbol{\omega}}_i\left(t_{k_i}^{\varphi i}\right) - \tilde{\boldsymbol{\omega}}_j\left(t_{k_j}^{\varphi j}\right)\right)\right\| + \varsigma_{\varphi 1}\right)} \quad (21)$$

where $0 < \alpha_\varphi < 1$, $\varsigma_{\varphi 1} > 0$, $\varsigma_{\varphi 2} = e^{c_{\varphi 1}\tanh(c_{\varphi 2}t)}$ with $c_{\varphi 1} > 0$, $c_{\varphi 2} > 0$, $t_{k_i}^{\varphi i}$ is the latest triggering instant of attitude dynamics, $\boldsymbol{e}_{\varphi i}(t) = \tilde{\boldsymbol{\omega}}_i(t_{k_i}^{\varphi i}) - \tilde{\boldsymbol{\omega}}_i(t)$, $t \in [t_{k_i}^{\varphi i}, t_{k_i+1}^{\varphi i})$ with $t_{k_i+1}^{\varphi i} := \inf\{t > t_{k_i}^{\varphi i} + \tau_{\min}^{\varphi i} | f_i(t, \boldsymbol{e}_{\varphi i}(t)) > 0\}$, where $\tau_{\min}^{\varphi i} \in \Re_{>0}$ is the lower-bound on inter-event time of attitude tracking.

Remark 3: Under the proposed event-triggered communication strategy, if $|e_{vi}(t)|$ and $\|\boldsymbol{e}_{\varphi i}(t)\|$ are greater than their corresponding thresholds, i.e., $f_i(t, e_{vi}(t)) > 0$, $f_i(t, \boldsymbol{e}_{\varphi i}(t)) > 0$, the communication is triggered, and the velocity and attitude information is allowed to broadcast to its neighbors. That is, there is no communication between the ith UAV and its neighbors during $t \in [t_{k_i}^{vi}, t_{k_i+1}^{vi})$ and $t \in [t_{k_i}^{\varphi i}, t_{k_i+1}^{\varphi i})$, which hence provides more efficient use of the communication network, however in turn, causes allowable degradation of control performance. More specific, decreasing c_{v1}, $c_{\varphi 1}$, c_{v2}, $c_{\varphi 2}$, α_v and α_φ can lead to more accurate tracking maneuvers, but at the cost of more communication resource. Conversely, increasing c_{v1}, $c_{\varphi 1}$, c_{v2}, $c_{\varphi 2}$, α_v and α_φ result in less communication consumption but larger tracking errors. Thus a compromise between the control performance and communication load should be made by choosing appropriate design parameters of c_{v1}, $c_{\varphi 1}$, c_{v2}, $c_{\varphi 2}$, α_v and α_φ.

Remark 4: Different from existing triggering mechanisms [14]–[18], wherein threshold parameters are permanently fixed, the specified thresholds of proposed triggering functions (20)–(21) are based on a state-dependent term and a time-dependent term. Specifically, the state-dependent term is constant in interevent interval unless its neighbors broadcast the new states to the ith UAV. While the time-dependent term initially increases and then keeps constant over time, which plays an important role in the elimination of Zeno behavior. Meanwhile, compared with the dynamic triggering rules for linearized dynamics of multi-agent system [22], [23] or linear cases of individual system [24], [25], our paper focuses on the multi-UAV system and integrates the exchange of velocity and attitude states into the

triggering functions, then proposes the novel dynamic triggering communication mechanisms for translational and rotational dynamics, respectively.

B. Controller Design and Stability Analysis

The event-based control protocol combines the communication triggering strategy within the coordinated controller design. Each UAV has three tasks: 1) Receiving the neighbors' latest transmitted information $\tilde{V}_j(t_{k_j}^{vj})$, $\tilde{\omega}_j(t_{k_j}^{\varphi j})$ and updating its controller immediately. 2) Monitoring its own state continuously and processing the triggered data with respect to every event-based condition. 3) Updating the controller and broadcasting the latest triggered data to the neighbors as soon as the event-based condition is satisfied. Based on above analysis, T_{xi0} and $\boldsymbol{\delta}_{i0}$ are constructed independently. The overall block diagram of proposed control scheme is depicted in Fig. 1.

1) Translational Kinematics: Noting (14), we obtain the derivative of $\tilde{V}_i$ as

$$\dot{\tilde{V}}_i = \frac{u_i T_{xi0}}{m_i V_i} + f_{vi} + \Delta_{vi} \quad (22)$$

where $f_{vi} = \frac{\boldsymbol{v}_i^{\mathrm{T}}}{V_i}(\boldsymbol{R}_1^{\mathrm{T}}(\boldsymbol{\varphi}_i)\boldsymbol{g} + \frac{\boldsymbol{F}_{i0}}{m_i}) - \dot{V}_r$.

To compensate the unknown disturbance Δ_{vi}, the disturbance observer is designed as

$$\begin{cases} \hat{\Delta}_{vi} = \hat{x}_{vi} + k_{i1}\tilde{V}_i \\ \dot{\hat{x}}_{vi} = -k_{i1}\left(\frac{u_i T_{xi0}}{m_i V_i} + f_{vi} + \hat{x}_{vi} + k_{i1}\tilde{V}_i\right) \end{cases} \quad (23)$$

where k_{i1} is a positive design parameter and $\hat{x}_{vi}$ is the state of disturbance observer.

With (23), the term $\hat{\Delta}_{vi}$ is the estimation of Δ_{vi}. The evolution of $\dot{\hat{\Delta}}_{vi}$ along (22)–(23) is described by

$$\dot{\hat{\Delta}}_{vi} = -k_{i1}\left(\frac{u_i T_{xi0}}{m_i V_i} + f_{vi} + \hat{x}_{vi} + k_{i1}\tilde{V}_i\right)$$
$$+ k_{i1}\left(\frac{u_i T_{xi0}}{m_i V_i} + f_{vi} + \Delta_{vi}\right) = k_{i1}\tilde{\Delta}_{vi} \quad (24)$$

where $\tilde{\Delta}_{vi} = \Delta_{vi} - \hat{\Delta}_{vi}$ denotes the estimation error of Δ_{vi}.

Consider the candidate Lyapunov function

$$L_1 = \frac{1}{2}\sum_{i=1}^{N}\tilde{V}_i^2 + \frac{1}{2}\sum_{i=1}^{N}\tilde{\Delta}_{vi}^2 \quad (25)$$

Taking the time derivative of (25) along (22) and (24) gives

$$\dot{L}_1 = \sum_{i=1}^{N}\tilde{V}_i\left(\frac{u_i T_{xi0}}{m_i V_i} + f_{vi} + \Delta_{vi}\right)$$
$$+ \sum_{i=1}^{N}\left(-k_{i1}\tilde{\Delta}_{vi}^2 + \tilde{\Delta}_{vi}\dot{\Delta}_{vi}\right) \quad (26)$$

Let us now design the control law T_{xi0} as follows

$$T_{xi0} = -\sigma_{vi}\frac{m_i V_i}{u_i}\sum_{j\in\mathcal{N}_i} a_{ij}\tanh\left(\tilde{V}_i\left(t_{k_i}^{vi}\right) - \tilde{V}_j\left(t_{k_j}^{vj}\right)\right)$$
$$- \frac{m_i V_i}{u_i}\left(k_{i2}\tilde{V}_i + f_{vi} + \hat{\Delta}_{vi}\right) \quad (27)$$

where σ_{vi}, k_{i2} are positive design parameters.

Theorem 1: Consider the translational kinematics (14) composed by the coordinated tracking controller (27) and disturbance observer (23). Let Assumptions 1 hold. There exist adjustable parameters k_{i1}, k_{i2} and σ_{vi} ($i = 1, 2, \ldots, N$) such that:

1) All signals of the translational subsystem are UUB in the presence of actuator faults, modeling uncertainties and external disturbances.
2) Velocity tracking error $\tilde{V}_i$ is guaranteed that $\lim_{t\to\infty}|\tilde{V}_i| \leq \mu_{Vi}$ with $\mu_{Vi} > 0$ a constant.
3) The communication burden for translational subsystem is considerably reduced. Meanwhile the Zeno phenomenon is precluded.

Proof: Substituting (27) into (26) and invoking Lemma 2, it follows that

$$
\begin{aligned}
\dot{L}_1 \leq &-\sum_{i=1}^{N} \sigma_{vi}\tilde{V}_i \sum_{j\in\mathcal{N}_i} a_{ij}\tanh\left(\tilde{V}_i\left(t_{k_i}^{vi}\right) - \tilde{V}_j\left(t_{k_j}^{vj}\right)\right)\\
&-\sum_{i=1}^{N} k_{i2}\tilde{V}_i^2 + \sum_{i=1}^{N} \tilde{V}_i\tilde{\Delta}_{vi} - \sum_{i=1}^{N}\left(k_{i1}\tilde{\Delta}_{vi}^2 - \tilde{\Delta}_{vi}\dot{\Delta}_{vi}\right)\\
= &\sum_{i=1}^{N} \sigma_{vi}e_{vi} \sum_{j\in\mathcal{N}_i} a_{ij}\tanh\left(\tilde{V}_i\left(t_{k_i}^{vi}\right) - \tilde{V}_j\left(t_{k_j}^{vj}\right)\right)\\
&-\frac{1}{2}\sum_{i=1}^{N} \sigma_{vi}\sum_{j\in\mathcal{N}_i} a_{ij}\left(\tilde{V}_i\left(t_{k_i}^{vi}\right)-\tilde{V}_j\left(t_{k_j}^{vj}\right)\right)\tanh\\
&\times\left(\tilde{V}_i\left(t_{k_i}^{vi}\right)-\tilde{V}_j\left(t_{k_j}^{vj}\right)\right) - \sum_{i=1}^{N} k_{i2}\tilde{V}_i^2 + \sum_{i=1}^{N}\tilde{V}_i\tilde{\Delta}_{vi}\\
&-\sum_{i=1}^{N}\left(k_{i1}\tilde{\Delta}_{vi}^2 - \tilde{\Delta}_{vi}\dot{\Delta}_{vi}\right)
\end{aligned}
\tag{28}
$$

Taking Lemma 3 into account, (28) further becomes

$$
\begin{aligned}
\dot{L}_1 \leq &\sum_{i=1}^{N} \sigma_{vi}|e_{vi}|\left|\sum_{j\in\mathcal{N}_i} a_{ij}\tanh\left(\tilde{V}_i\left(t_{k_i}^{vi}\right) - \tilde{V}_j\left(t_{k_j}^{vj}\right)\right)\right|\\
&-\frac{1}{2}\sum_{i=1}^{N} \sigma_{vi}\sum_{j\in\mathcal{N}_i} a_{ij}\left|\tanh\left(\tilde{V}_i\left(t_{k_i}^{vi}\right) - \tilde{V}_j\left(t_{k_j}^{vj}\right)\right)\right|^2\\
&-\sum_{i=1}^{N} k_{i2}\tilde{V}_i^2 + \sum_{i=1}^{N}\tilde{V}_i\tilde{\Delta}_{vi} - \sum_{i=1}^{N}\left(k_{i1}\tilde{\Delta}_{vi}^2 - \tilde{\Delta}_{vi}\dot{\Delta}_{vi}\right)
\end{aligned}
\tag{29}
$$

Under the proposed event-triggered communication strategy, $f_i(t, e_{vi}(t)) \leq 0$ holds during $t \in [t_{k_i}^{vi}, t_{k_i+1}^{vi})$, that is

$$
|e_{vi}| \leq \frac{\alpha_v\sum_{j\in\mathcal{N}_i} a_{ij}\left|\tanh\left(\tilde{V}_i\left(t_{k_i}^{vi}\right) - \tilde{V}_j\left(t_{k_j}^{vj}\right)\right)\right|^2}{2\left(\left|\sum_{j\in\mathcal{N}_i} a_{ij}\tanh\left(\tilde{V}_i\left(t_{k_i}^{vi}\right) - \tilde{V}_j\left(t_{k_j}^{vj}\right)\right)\right| + \varsigma_{v1}\right)} + \varsigma_{v2}
\tag{30}
$$

Substituting (30) into (29) yields

$$
\begin{aligned}
\dot{L}_1 \leq &\frac{\alpha_v - 1}{2}\sum_{i=1}^{N} \sigma_{vi}\sum_{j\in\mathcal{N}_i} a_{ij}\left(\left|\tanh\left(\tilde{V}_i\left(t_{k_i}^{vi}\right) - \tilde{V}_j\left(t_{k_j}^{vj}\right)\right)\right|\right.\\
&\left.-\frac{\varsigma_{v2}}{1-\alpha_v}\right)^2 + \frac{\varsigma_{v2}^2}{2(1-\alpha_v)}\sum_{i=1}^{N} \sigma_{vi}\sum_{j\in\mathcal{N}_i} a_{ij} - \sum_{i=1}^{N} k_{i2}\tilde{V}_i^2\\
&+\sum_{i=1}^{N} \tilde{V}_i\tilde{\Delta}_{vi} - \sum_{i=1}^{N}\left(k_{i1}\tilde{\Delta}_{vi}^2 - \tilde{\Delta}_{vi}\dot{\Delta}_{vi}\right)\\
\leq &-\sum_{i=1}^{N} k_{i2}\tilde{V}_i^2 + \sum_{i=1}^{N}\tilde{V}_i\tilde{\Delta}_{vi} - \sum_{i=1}^{N}\left(k_{i1}\tilde{\Delta}_{vi}^2 - \tilde{\Delta}_{vi}\dot{\Delta}_{vi}\right)\\
&+\frac{\varsigma_{v2}^2}{2(1-\alpha_v)}\sum_{i=1}^{N} \sigma_{vi}\sum_{j\in\mathcal{N}_i} a_{ij}
\end{aligned}
\tag{31}
$$

Using Young's inequality, it can be checked that

$$
\begin{aligned}
\dot{L}_1 \leq &-\sum_{i=1}^{N}\left(k_{i2} - \frac{1}{2}\right)\tilde{V}_i^2 - \sum_{i=1}^{N}(k_{i1} - 1)\tilde{\Delta}_{vi}^2\\
&+\sum_{i=1}^{N} \frac{1}{2}\dot{\Delta}_{vi}^2 + \frac{\varsigma_{v2}^2}{2(1-\alpha_v)}\sum_{i=1}^{N} \sigma_{vi}\sum_{j\in\mathcal{N}_i} a_{ij}\\
\leq &-\kappa_{vi}L_1 + \chi_{vi}
\end{aligned}
\tag{32}
$$

where from the boundedness of ρ_{T_i}, $\boldsymbol{v}_i$, T_{xi0}, T_{xif}, $\Delta\boldsymbol{F}_i$ and $\boldsymbol{d}_{vi}$, there exists a positive constant $\overline{\Delta}_{vi}$ such that $|\dot{\Delta}_{vi}| \leq \overline{\Delta}_{vi}$. It can be concluded that $\kappa_{vi} = \min\{2k_{i2} - 1, 2k_{i1} - 2\}$ with $k_{i1} > 1$, $k_{i2} > \frac{1}{2}$, $\chi_{vi} = \frac{1}{2}\sum_{i=1}^{N}\overline{\Delta}_{vi}^2 + \frac{\varsigma_{v2}^2}{2(1-\alpha_{v2})}\sum_{i=1}^{N}\sigma_{vi}\sum_{j\in\mathcal{N}_i} a_{ij}$.

Integrating (32) over $[0, t]$ leads to

$$
0 \leq L_1 \leq \left[\frac{\chi_{vi}}{\kappa_{vi}} + L_1(0)\right]e^{-\kappa_{vi}t} + \frac{\chi_{vi}}{\kappa_{vi}}
\tag{33}
$$

As a result, all closed-loop signals in translational dynamics are UUB. Next, we prove that no Zeno behavior exhibits during maneuvers. That is, there exists a $t_v^* > 0$ satisfying $\{t_{k_i+1}^{vi} - t_{k_i}^{vi}\} \geq t_v^*$. Recalling the definition of $e_{vi}(t)$, the evolution of $|e_{vi}(t)|$ over the time interval $t \in [t_{k_i}^{\varphi i}, t_{k_i+1}^{\varphi i})$ satisfies

$$
\frac{d}{dt}|e_{vi}| \leq \left|\frac{d}{dt}\left(\tilde{V}_i\left(t_{k_i}^{vi}\right) - \tilde{V}_i(t)\right)\right| = \left|\dot{\tilde{V}}_i(t)\right|
\tag{34}
$$

$\dot{\tilde{V}}_i(t)$ has been proved bounded in previous analysis. Therefore, there exists a positive constant μ_{vi} such that $|\dot{\tilde{V}}_i(t)| \leq \mu_{vi}$. Since $e_{vi}(t_{k_i}^{vi}) = 0$, we see that $|e_{vi}| \leq \mu_{vi}t_v^*$. Further, we have

$$
\frac{\alpha_v\sum_{j\in\mathcal{N}_i} a_{ij}\left|\tanh\left(\tilde{V}_i\left(t_{k_i}^{vi}\right) - \tilde{V}_j\left(t_{k_j}^{vj}\right)\right)\right|^2}{2\left(\left|\sum_{j\in\mathcal{N}_i} a_{ij}\tanh\left(\tilde{V}_i\left(t_{k_i}^{vi}\right) - \tilde{V}_j\left(t_{k_j}^{vj}\right)\right)\right| + \varsigma_{v1}\right)} + \varsigma_{v2} \leq \mu_{vi}t_v^*
\tag{35}
$$

From (35), $\mu_{vi}t_v^* \geq \varsigma_{v2}$ holds. Additionally, considering $1 \leq \varsigma_{v2} \leq e^{c_{v1}}$, it is verified that $t_v^* \geq 1/\mu_{vi} > 0$. Clearly, the Zeno behavior is successfully avoided.

This completes the proof of Theorem 1.

Remark 5: It should be noticed that $\tilde{V}_i$ can be made arbitrarily small by increasing k_{i1}, k_{i2} and σ_{vi}. Moreover, the choice of c_{v1}, c_{v2} and α_v should balance the control performance and triggering number of communication. This will be shown in the following numerical example.

Remark 6: Compared with the cooperative controllers of UAVs containing continuous exchanges of state information among neighbors [8]–[14], the proposed T_{xi0} only uses the neighbors state $\tilde{V}_j(t_{k_j}^{vj})$ in control protocol (27) at event-triggered instants, which greatly reduces the communication burden during $t \in [t_{k_j}^{vj}, t_{k_{j+1}}^{vj})$.

2) Rotational Kinematics: The rotational control design comprises two steps:

Step 1: Taking the time derivative of $\frac{1}{2}\sum_{i=1}^{N} \tilde{\varphi}_i^{\mathrm{T}} \tilde{\varphi}_i$ along (3) yields

$$\sum_{i=1}^{N} \tilde{\varphi}_i^{\mathrm{T}} \dot{\tilde{\varphi}}_i = \sum_{i=1}^{N} \tilde{\varphi}_i^{\mathrm{T}} \left[R_2^{-1} \left(\tilde{\omega}_i + \omega_{di} \right) - \dot{\varphi}_r \right] \quad (36)$$

We design the intermediate control signal as

$$\omega_{di} = R_2 \left(-K_{i1} \tilde{\varphi}_i + \dot{\varphi}_r \right) \quad (37)$$

where $K_{i1} \in \Re^{3 \times 3}$ is symmetric and positive definite.

Substituting (37) into (36) leads to

$$\sum_{i=1}^{N} \tilde{\varphi}_i^{\mathrm{T}} \dot{\tilde{\varphi}}_i = \sum_{i=1}^{N} \left(-\tilde{\varphi}_i^{\mathrm{T}} K_{i1} \tilde{\varphi}_i + \tilde{\varphi}_i^{\mathrm{T}} R_2^{-1} \tilde{\omega}_i \right) \quad (38)$$

Step 2: For the purpose of forcing ω_i to track ω_{di}, from (17), it holds that

$$J_{i0} \dot{\tilde{\omega}}_i = -\omega_i \times J_{i0} \omega_i + N_{i0} + C_{i0} \delta_{i0} + \Delta_{\omega i} - J_{i0} \dot{\omega}_{di}$$
$$= G_i + C_{i0} \delta_{i0} + \Delta_{\omega i} \quad (39)$$

where $G_i = -\omega_i \times J_{i0} \omega_i + N_{i0} - J_{i0} \dot{\omega}_{di}$.

To estimate the lumped disturbance $\Delta_{\omega i}$, design the disturbance observer as

$$\begin{cases} \hat{\Delta}_{\omega i} = \hat{x}_{\omega i} + K_{i2} \tilde{\omega}_i \\ \dot{\hat{x}}_{\omega i} = -K_{i2} J_{i0}^{-1} \left(G_i + C_{i0} \delta_{i0} + \hat{x}_{\omega i} + K_{i2} \tilde{\omega}_i \right) \end{cases} \quad (40)$$

where $K_{i2} \in \Re^{3 \times 3}$ is symmetric and positive definite. $\hat{x}_{\omega i} = [\hat{x}_{\omega 1}, \hat{x}_{\omega 2}, \hat{x}_{\omega 3}]^{\mathrm{T}}$ is the state of proposed disturbance observer.

Taking the time derivative of (40), one has

$$\dot{\hat{\Delta}}_{\omega i} = -K_{i2} J_{i0}^{-1} \left(G_i + C_{i0} \delta_{i0} + \hat{x}_{\omega i} + K_{i2} \tilde{\omega}_i \right)$$
$$+ K_{i2} J_{i0}^{-1} \left(G_i + C_{i0} \delta_{i0} + \Delta_{\omega i} \right) = K_{i2} J_{i0}^{-1} \tilde{\Delta}_i \quad (41)$$

where $\tilde{\Delta}_{\omega i} = \Delta_{\omega i} - \hat{\Delta}_{\omega i}$ is the estimation error of $\Delta_{\omega i}$.

Take the candidate Lyapunov function as

$$L_2 = \frac{1}{2} \sum_{i=1}^{N} \tilde{\varphi}_i^{\mathrm{T}} \tilde{\varphi}_i + \frac{1}{2} \sum_{i=1}^{N} \tilde{\omega}_i^{\mathrm{T}} J_{i0} \tilde{\omega}_i + \frac{1}{2} \sum_{i=1}^{N} \tilde{\Delta}_{\omega i}^{\mathrm{T}} J_{i0} \tilde{\Delta}_{\omega i} \quad (42)$$

From (38), (39), and (41), taking the time derivative of L_2 leads to

$$\dot{L}_2 = \sum_{i=1}^{N} \left(-\tilde{\varphi}_i^{\mathrm{T}} K_{i1} \tilde{\varphi}_i + \tilde{\varphi}_i^{\mathrm{T}} R_2^{-1} \tilde{\omega}_i \right)$$

$$+ \sum_{i=1}^{N} \tilde{\omega}_i^{\mathrm{T}} \left(G_i + C_{i0} \delta_{i0} + \Delta_{\omega i} \right)$$

$$- \sum_{i=1}^{N} \left(\tilde{\Delta}_{\omega i}^{\mathrm{T}} K_{i2} \tilde{\Delta}_{\omega i} - \tilde{\Delta}_{\omega i}^{\mathrm{T}} J_{i0} \dot{\Delta}_{\omega i} \right) \quad (43)$$

Design the event-based coordinated controller as

$$\delta_{i0} = -\sigma_{\varphi i} C_{i0}^{-1} \sum_{j \in \mathcal{N}_i} a_{ij} \tanh \left(\tilde{\omega}_i \left(t_{k_i}^{\varphi i} \right) - \tilde{\omega}_j \left(t_{k_j}^{\varphi j} \right) \right)$$

$$- C_{i0}^{-1} \left(K_{i3} \tilde{\omega}_i + \left(R_2^{-1} \right)^{\mathrm{T}} \tilde{\varphi}_i + G_i + \hat{\Delta}_{\omega i} \right) \quad (44)$$

where $\sigma_{\varphi i}$ is a positive design parameter and $K_{i3} \in \Re^{3 \times 3}$ is a symmetric positive definite matrix.

Theorem 2: Consider the rotational kinematics (3), (17) composed by the coordinated tracking controller (44) and disturbance observer (40). Let Assumptions 1 hold. There exist adjustable parameters K_{i1}, K_{i2}, K_{i3}, $\sigma_{\varphi i}$, $(i = 1, 2, \ldots, N)$ such that:

1) All signals of the rotational subsystem are UUB in the presence of actuator faults, modeling uncertainties and external disturbances.
2) Attitude tracking error $\tilde{\varphi}_i$ is guaranteed that $\lim_{t \to \infty} \|\tilde{\varphi}_i\| \leq \mu_{\varphi i}$ with $\mu_{\varphi i} > 0$ a constant.
3) The communication burden for rotational subsystem is considerably reduced. Meanwhile the Zeno phenomenon is avoided.

Proof: Substituting the controller (44) into (43) gives

$$\dot{L}_2 = -\sum_{i=1}^{N} \sigma_{\varphi i} \tilde{\omega}_i^{\mathrm{T}} \sum_{j \in \mathcal{N}_i} a_{ij} \tanh \left(\tilde{\omega}_i \left(t_{k_i}^{\varphi i} \right) - \tilde{\omega}_j \left(t_{k_j}^{\varphi j} \right) \right)$$

$$- \sum_{i=1}^{N} \tilde{\varphi}_i^{\mathrm{T}} K_{i1} \tilde{\varphi}_i - \sum_{i=1}^{N} \tilde{\omega}_i^{\mathrm{T}} K_{i3} \tilde{\omega}_i + \sum_{i=1}^{N} \tilde{\omega}_i^{\mathrm{T}} \tilde{\Delta}_{\omega i}$$

$$- \sum_{i=1}^{N} \left(\tilde{\Delta}_{\omega i}^{\mathrm{T}} K_{i2} \tilde{\Delta}_{\omega i} - \tilde{\Delta}_{\omega i}^{\mathrm{T}} J_{i0} \dot{\Delta}_{\omega i} \right) \quad (45)$$

By invoking Lemma 2 and Lemma 3, whereby (45) can be rewritten as

$$\dot{L}_2 \leq \sum_{i=1}^{N} \sigma_{\varphi i} \|e_{\varphi i}\| \left\| \sum_{j \in \mathcal{N}_i} a_{ij} \tanh \left(\tilde{\omega}_i \left(t_{k_i}^{\varphi i} \right) - \tilde{\omega}_j \left(t_{k_j}^{\varphi j} \right) \right) \right\|$$

$$- \frac{1}{2} \sum_{i=1}^{N} \sigma_{\varphi i} \sum_{j \in \mathcal{N}_i} a_{ij} \left\| \tanh \left(\tilde{\omega}_i \left(t_{k_i}^{\varphi i} \right) - \tilde{\omega}_j \left(t_{k_j}^{\varphi j} \right) \right) \right\|^2$$

$$- \sum_{i=1}^{N} \tilde{\varphi}_i^{\mathrm{T}} K_{i1} \tilde{\varphi}_i - \sum_{i=1}^{N} \tilde{\omega}_i^{\mathrm{T}} K_{i3} \tilde{\omega}_i + \sum_{i=1}^{N} \tilde{\omega}_i^{\mathrm{T}} \tilde{\Delta}_{\omega i}$$

$$- \sum_{i=1}^{N} \left(\tilde{\Delta}_{\omega i}^{\mathrm{T}} K_{i2} \tilde{\Delta}_{\omega i} - \tilde{\Delta}_{\omega i}^{\mathrm{T}} J_{i0} \dot{\Delta}_{\omega i} \right) \quad (46)$$

Under proposed event-triggered communication mechanism, $f_i(t, e_{\varphi i}(t)) \leq 0$ satisfies in the interval $t \in [t_{k_i}^{\varphi i}, t_{k_i+1}^{\varphi i})$, that is

$$\|e_{\varphi i}\| \leq \frac{\alpha_\varphi \sum_{j \in \mathcal{N}_i} a_{ij} \left\| \tanh\left(\tilde{\omega}_i\left(t_{k_i}^{\varphi i}\right) - \tilde{\omega}_j\left(t_{k_j}^{\varphi j}\right)\right) \right\|^2}{2\left(\left\|\sum_{j \in \mathcal{N}_i} a_{ij} \tanh\left(\tilde{\omega}_i\left(t_{k_i}^{\varphi i}\right) - \tilde{\omega}_j\left(t_{k_j}^{\varphi j}\right)\right)\right\| + \varsigma_{\varphi 1}\right)} + \varsigma_{\varphi 2} \quad (47)$$

Inserting (47) into (46), we have

$$\dot{L}_2 \leq \frac{\alpha_\varphi - 1}{2} \sum_{i=1}^N \sigma_{\varphi i} \sum_{j \in \mathcal{N}_i} a_{ij} \left(\left\| \tanh\left(\tilde{\omega}_i\left(t_{k_i}^{\varphi i}\right) - \tilde{\omega}_j\left(t_{k_j}^{\varphi j}\right)\right) \right\| \right.$$
$$\left. - \frac{\varsigma_{\varphi 2}}{1 - \alpha_\varphi}\right)^2 + \frac{\varsigma_{\varphi 2}^2}{2(1 - \alpha_\varphi)} \sum_{i=1}^N \sigma_{\varphi i} \sum_{j \in \mathcal{N}_i} a_{ij}$$
$$- \sum_{i=1}^N \tilde{\varphi}_i^{\mathrm{T}} K_{i1} \tilde{\varphi}_i - \sum_{i=1}^N \tilde{\omega}_i^{\mathrm{T}} K_{i3} \tilde{\omega}_i + \sum_{i=1}^N \tilde{\omega}_i^{\mathrm{T}} \tilde{\Delta}_{\omega i}$$
$$- \sum_{i=1}^N \left(\tilde{\Delta}_{\omega i}^{\mathrm{T}} K_{i2} \tilde{\Delta}_{\omega i} - \tilde{\Delta}_{\omega i}^{\mathrm{T}} J_{i0} \dot{\Delta}_{\omega i}\right)$$
$$\leq - \sum_{i=1}^N \tilde{\varphi}_i^{\mathrm{T}} K_{i1} \tilde{\varphi}_i - \sum_{i=1}^N \tilde{\omega}_i^{\mathrm{T}} K_{i3} \tilde{\omega}_i + \sum_{i=1}^N \tilde{\omega}_i^{\mathrm{T}} \tilde{\Delta}_{\omega i}$$
$$- \sum_{i=1}^N \left(\tilde{\Delta}_{\omega i}^{\mathrm{T}} K_{i2} \tilde{\Delta}_{\omega i} - \tilde{\Delta}_{\omega i}^{\mathrm{T}} J_{i0} \dot{\Delta}_{\omega i}\right)$$
$$+ \frac{\varsigma_{\varphi 2}^2}{2(1 - \alpha_\varphi)} \sum_{i=1}^N \sigma_{\varphi i} \sum_{j \in \mathcal{N}_i} a_{ij} \quad (48)$$

Rearranging (48) gives

$$\dot{L}_2 \leq - \sum_{i=1}^N \lambda_{\min}(K_{i1}) \tilde{\varphi}_i^{\mathrm{T}} \tilde{\varphi}_i - \sum_{i=1}^N \left(\lambda_{\min}(K_{i3}) - \frac{1}{2}\right) \tilde{\omega}_i^{\mathrm{T}} \tilde{\omega}_i$$
$$+ \sum_{i=1}^N \frac{\lambda_{\max}(J_{i0})}{2} \dot{\Delta}_{\omega i}^{\mathrm{T}} \dot{\Delta}_{\omega i} + \frac{\varsigma_{\varphi 2}^2}{2(1 - \alpha_\varphi)} \sum_{i=1}^N \sigma_{\varphi i} \sum_{j \in \mathcal{N}_i} a_{ij}$$
$$- \sum_{i=1}^N \left(\lambda_{\min}(K_{i2}) - \frac{\lambda_{\max}(J_{i0}) + 1}{2}\right) \tilde{\Delta}_{\omega i}^{\mathrm{T}} \tilde{\Delta}_{\omega i}$$
$$\leq - \kappa_{\omega i} L_2 + \chi_{\omega i} \quad (49)$$

where from the boundedness of ΔJ_i, $\dot{\omega}_i$, ω_i, ΔN_i, δ_{if}, C_{i0}, ρ_i, δ_{i0}, ΔC_i and $d_{\omega i}$, there exists a positive constant $\overline{\Delta}_{\omega i}$ such that $\|\dot{\Delta}_{\omega i}\| \leq \overline{\Delta}_{\omega i}$. It can be obtained that $\kappa_{\omega i} = \min\{2\lambda_{\min}(K_{i1}), \frac{2\lambda_{\min}(K_{i3}) - 1}{\lambda_{\max}(J_{i0})}, \frac{2\lambda_{\min}(K_{i2}) - 1}{\lambda_{\max}(J_{i0})} - 1\}$ with K_{i2} and K_{i3} satisfying $\lambda_{\min}(K_{i2}) > \frac{\lambda_{\max}(J_{i0}) + 1}{2}$, $\lambda_{\min}(K_{i3}) > \frac{1}{2}$, and $\chi_{\omega i} = \sum_{i=1}^N \frac{\lambda_{\max}(J_{i0})}{2} \overline{\Delta}_{\omega i}^2 + \frac{\varsigma_{\varphi 2}^2}{2(1 - \alpha_\varphi)} \sum_{i=1}^N \sigma_{\varphi i} \sum_{j \in \mathcal{N}_i} a_{ij}$.

Integrating (49) over $[0, t]$ yields

$$0 \leq L_2 \leq \left[\frac{\chi_{\omega i}}{\kappa_{\omega i}} + L_2(0)\right] e^{-\kappa_{\omega i} t} + \frac{\chi_{\omega i}}{\kappa_{\omega i}} \quad (50)$$

As a result, all closed-loop signals of rotational subsystem are UUB. Further it is proved that the Zeno behavior can be avoided. That is, there exists a $t_\varphi^* > 0$ satisfying $\{t_{k_i+1}^{\varphi i} - t_{k_i}^{\varphi i}\} \geq t_\varphi^*$. Considering the definition of $e_{\varphi i}$, differentiating $\|e_{\varphi i}\|$ over time interval $t \in [t_{k_i}^{\varphi i}, t_{k_i+1}^{\varphi i})$ yields

$$\frac{d}{dt} \|e_{\varphi i}(t)\| \leq \left\| \frac{d}{dt}\left(\tilde{\omega}_i\left(t_{k_i}^{\varphi i}\right) - \tilde{\omega}_i(t)\right)\right\| = \|\dot{\tilde{\omega}}_i(t)\| \quad (51)$$

$\dot{\tilde{\omega}}_i(t)$ has been proved bounded based on previous analysis. Therefore, there exists a positive constant $\mu_{\varphi i}$ such that $\|\dot{\tilde{\omega}}_i(t)\| \leq \mu_{\varphi i}$. Since $\|e_{\varphi i}(t_{k_i}^{\varphi i})\| = 0$, we obtain that $\|e_{\varphi i}(t)\| \leq \mu_{\varphi i} t_\varphi^*$. In view of (47), there exists

$$\frac{\alpha_\varphi \sum_{j \in \mathcal{N}_i} a_{ij} \left\| \tanh\left(\tilde{\omega}_i\left(t_{k_i}^{\varphi i}\right) - \tilde{\omega}_j\left(t_{k_j}^{\varphi j}\right)\right) \right\|^2}{2\left(\left\|\sum_{j \in \mathcal{N}_i} a_{ij} \tanh\left(\tilde{\omega}_i\left(t_{k_i}^{\varphi i}\right) - \tilde{\omega}_j\left(t_{k_j}^{\varphi j}\right)\right)\right\| + \varsigma_{\varphi 1}\right)} + \varsigma_{\varphi 2} \leq \mu_{\varphi i} t_\varphi^* \quad (52)$$

From (52), there exists $\mu_{\varphi i} t_\varphi^* \geq \varsigma_{\varphi 2}$. Therefore, with $1 \leq \varsigma_{\varphi 2} \leq e^{c_{\varphi 1}}$, it is verified that $t_\varphi^* \geq 1/\mu_{\varphi i} > 0$. Clearly, the Zeno behavior is successfully precluded.

This completes the proof of Theorem 2.   ■

Remark 7: Note that $\|\tilde{\varphi}_i\|$ can be made arbitrarily small by increasing K_{i1}, K_{i2}, K_{i3} and $\sigma_{\varphi i}$. Moreover, a good balance of convergence performance and triggering number of communication should be made by choosing reasonable parameters $c_{\varphi 1}$, $c_{\varphi 2}$ and α_φ. This will be further shown in the following numerical simulation.

Remark 8: Different from existing results [8]–[14] with the continuous state information exchanges among neighboring UAVs in controller design, our proposed δ_{i0} simply uses discrete neighbors' state $\tilde{\omega}_j(t_{k_j}^{\varphi j})$ in control protocol (44), which lightens the communication exchange during $t \in [t_{k_j}^{\varphi j}, t_{k_j+1}^{\varphi j})$.

Remark 9: Compared with existing literature [28], [35]–[37], [38] using neural networks learning mechanisms to cope with lumped uncertainties caused by actuator faults, external disturbances and model uncertainties, the proposed disturbance observer compensates for compounded disturbances with less online learning parameters and simpler internal structure, thus reducing the computation burden and obtaining faster disturbance estimation. As a result, the designed disturbance observer is more applicable to disturbance rejection for practical UAV system.

IV. SIMULATION RESULTS AND ANALYSIS

A. Simulation Scenarios

To verify the effectiveness of proposed scheme, a simulation scenario is considered to address a coordinated tracking problem for three networked fixed-wing UAVs. The structure parameters and coefficient values of each UAV are list in Table I [29]. While the corresponding communication topology is illustrated in Fig. 3. The initial conditions are summarized as $V_{10} = V_{20} = V_{30} = 20\text{m/s}$, $\varphi_{10} = [0°, 1°, 0°]^{\mathrm{T}}$, $\varphi_{20} = \varphi_{30} = [0.5°, 1°, 0.5°]^{\mathrm{T}}$ and $\omega_{10} = \omega_{20} = \omega_{30} = [0, 0, 0]^{\mathrm{T}} \text{rad/s}$. Suppose that the external disturbances in velocity and attitude motion are described as $d_{v1} = d_{v2} = $
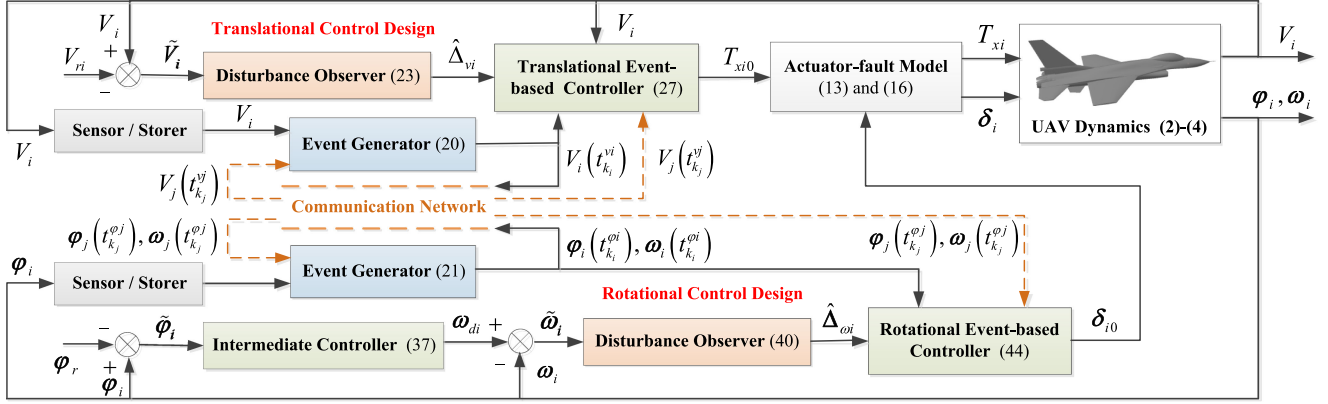
Fig. 2. Overall framework of the proposed control strategy.

TABLE I
STRUCTURAL AND AERODYNAMIC PARAMETER VALUES OF UAV

Coefficient	Value	Unit	Coefficient	Value	Unit
m_i	20.64	kg	b_i	1.96	m
S_i	1.37	m^2	$\bar{c}_i$	0.76	m
ρ	1.29	$\mathrm{kg \cdot m}^{-3}$	g	9.8	$\mathrm{m \cdot s}^{-2}$
J_{xi}	1.607	$\mathrm{kg \cdot m}^2$	J_{yi}	7.51	$\mathrm{kg \cdot m}^2$
J_{zi}	7.18	$\mathrm{kg \cdot m}^2$	J_{xzi}	0.59	$\mathrm{kg \cdot m}^2$
c_{L0i}	0.1	/	$c_{L\alpha_i}$	0.25	rad^{-1}
c_{D0i}	0.5	/	$c_{Y\beta_i}$	−0.1	rad^{-1}
c_{l0i}	−0.001	/	$c_{l\beta_i}$	−0.038	rad^{-1}
c_{lpi}	−0.213	$\mathrm{rad}^{-1} \cdot \mathrm{s}$	c_{lri}	0.114	$\mathrm{rad}^{-1} \cdot \mathrm{s}$
$c_{l\delta_{ai}}$	−0.056	rad^{-1}	$c_{l\delta_{ri}}$	0.014	rad^{-1}
c_{m0i}	0.022	/	$c_{m\alpha_i}$	−0.473	rad^{-1}
c_{mqi}	−3.449	$\mathrm{rad}^{-1} \cdot \mathrm{s}$	$c_{m\delta_{ei}}$	−0.364	rad^{-1}
c_{n0i}	0.022	/	$c_{n\beta_i}$	0.036	rad^{-1}
c_{npi}	−0.151	$\mathrm{rad}^{-1} \cdot \mathrm{s}$	c_{nri}	−0.195	$\mathrm{rad}^{-1} \cdot \mathrm{s}$
$c_{n\delta_{ai}}$	−0.036	rad^{-1}	$c_{n\delta_{ri}}$	−0.055	rad^{-1}
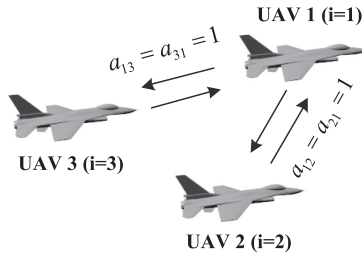
Fig. 3. Communication topology.

$\boldsymbol{d}_{v3} = [0.3\sin(t), 0.5\cos(2t), 0.2\cos(t)]^{\mathrm{T}}$ and $\boldsymbol{d}_{\omega 2} = \boldsymbol{d}_{\omega 3} = [0.3\cos(2t), 0.2\sin(3t), 0.5\sin(t)]^{\mathrm{T}}$. Meanwhile, the actuator faults are introduced in velocity channel as $\rho_{T_3} = 0.9$ during $t \in (2, 5]$s. Assume that the virtual leader UAV is to complete low altitude penetration mission and track the desired trajectory as

$$V_r = \begin{cases} 20 + \frac{30}{2s+1}, & 0s \le t < 7s \\ 20 + \frac{20}{0.4s+1}, & 7s \le t \le 12s \\ 20 + \frac{40}{0.4s+1}, & t > 12s \end{cases}$$

$$\varphi_r = \begin{cases} [0,0,0]^{\mathrm{T}}, & 0s \le t < 5s \\ [0, \frac{-10}{0.1s+1}, 0]^{\mathrm{T}}, & 5s \le t \le 15s \\ [0,0,0]^{\mathrm{T}}, & t > 15s \end{cases}$$

The controllers and disturbance observers are provided by (23), (27), (40), (44) with design parameters as $\alpha_v = 0.5$, $\varsigma_{v1} = 0.1$, $c_{v1} = 0.1$, $c_{v2} = 0.2$, $\sigma_{v1} = \sigma_{v2} = 10(0\ s \le t \le 12\ s); 100(12\ s < t \le 14\ s); 150(t > 14\ s)$, $\sigma_{v3} = 10(0\ s \le t \le 12\ s); 100(12\ s < t \le 14\ s); 10(t > 14\ s)$, $k_{11} = k_{21} = k_{31} = 0.02(0\ s \le t \le 14\ s); 0.002(t > 14\ s)$, $k_{12} = k_{22} = k_{32} = 10(0\ s \le t \le 5\ s); 100(5\ s < t \le 12\ s); 20(12\ s < t \le 14\ s); 100(t > 14\ s)$, $\alpha_\varphi = 0.5$, $\varsigma_{\varphi 1} = 0.1$, $c_{\varphi 1} = 0.1$, $c_{\varphi 2} = 0.2$, $\sigma_{\varphi 1} = \sigma_{\varphi 2} = \sigma_{\varphi 3} = 1$, $\boldsymbol{K}_{11} = \boldsymbol{K}_{21} = \boldsymbol{K}_{31} = \boldsymbol{K}_{12} = \boldsymbol{K}_{22} = \boldsymbol{K}_{32} = \mathrm{diag}\{1,1,1\}$, $\boldsymbol{K}_{13} = \boldsymbol{K}_{23} = \boldsymbol{K}_{33} = \mathrm{diag}\{50,60,50\}$.

To comprehensively highlight the performance of proposed approach, three situations are presented and discussed. The first case verifies the efficiency of proposed controller based on the above simulation scenario. The second one illustrates the superiority of dynamic event-triggered communication mechanism (DECM) over the periodic communication mechanism (PCM) and static event-triggered communication mechanism (SECM). The last case evaluates the sensitivity of proposed event-triggered conditions for different fault modes.

B. Results and Analysis

Case 1: In this case, the proposed controller is conducted based on above simulation scenario. Fig. 4 shows the trajectories of velocities and attitudes for the multi-UAV system. From Fig. 4(a)–(d), it can be observed that the velocities and attitudes both converge availably to their desired trajectories, which validates the effectiveness of proposed control scheme. Additionally, the tracking errors of velocities and attitudes are depicted in Fig. 4(e)–(h). The data release intervals and broadcasting instants of velocity and attitude for each UAV are presented in Fig. 5 and Fig. 6. Obviously, the communication among UAVs is intermittent, meanwhile no Zeno behavior exhibits. Thus we can see that the proposed event-based control scheme can maintain the expected tracking performances of velocities and attitudes despite the presence of actuator faults and external disturbances.

Case 2: To illustrate the advantages of event-triggered strategy in terms of DECM, two other communication mechanisms are evaluated in this comparative study: i) PCM: information exchanges among neighboring UAVs are performed in a periodic manner. ii) SECM: different from DECM in (20) and
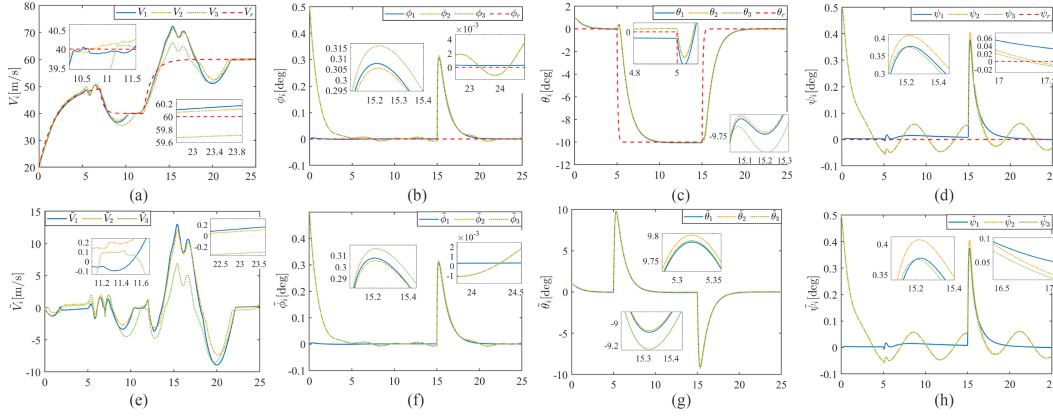
Fig. 4. Velocity and attitude tracking of multiple UAVs by proposed controller. (a)–(h) show the curves of state responses and errors. (a) Velocity response (b) Roll angle response (c) Pitch angle response (d) Yaw angle response (e) Tracking error of velocity (f) Tracking error of roll angle (g) Tracking error of pitch angle (h) Tracking error of yaw angle.
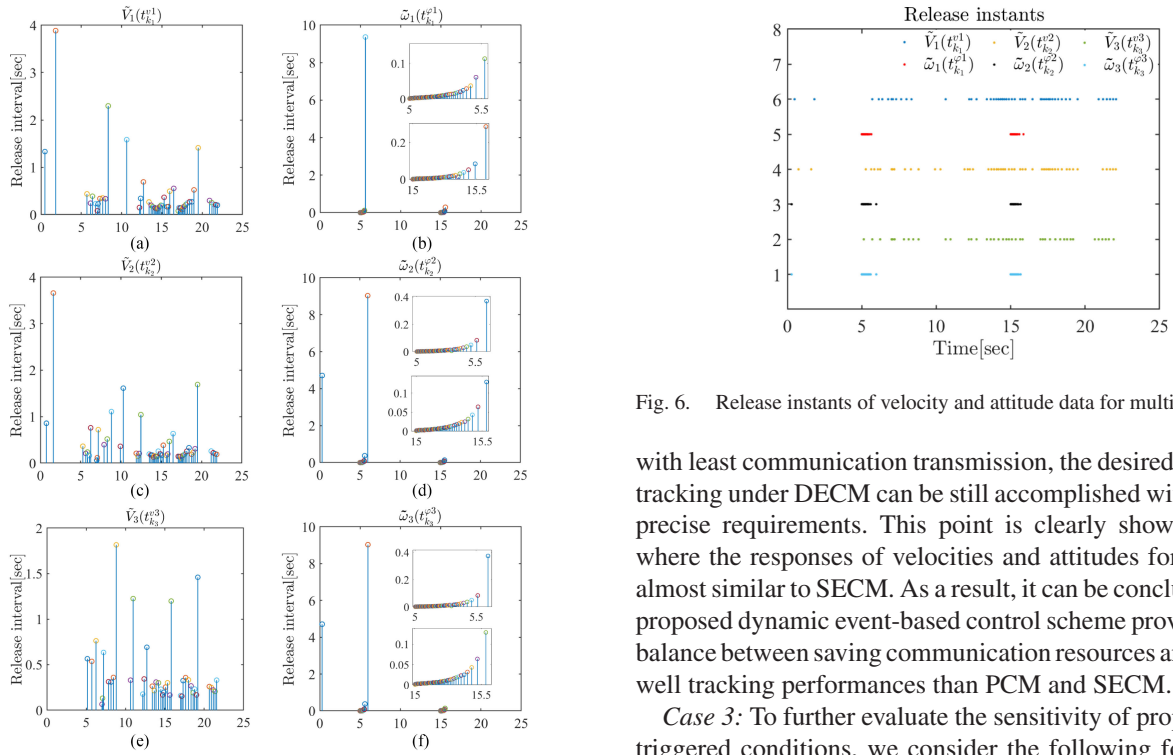

Fig. 5. Release intervals of velocity and attitude data for multi-UAV system. (a)–(f) show the curves of release intervals. (a) Data $\tilde{V}_1(t_{k_1}^{v1})$ (b) Data $\tilde{\omega}_1(t_{k_1}^{\varphi1})$ (c) Data $\tilde{V}_2(t_{k_2}^{v2})$ (d) Data $\tilde{\omega}_2(t_{k_2}^{\varphi2})$ (e) Data $\tilde{V}_3(t_{k_3}^{v3})$ (f) Data $\tilde{\omega}_3(t_{k_3}^{\varphi3})$.

Fig. 6. Release instants of velocity and attitude data for multi-UAV system.

(21), the threshold parameter in SECM is fixed permanently as [20]. That is, $f_i(t, e_{vi}(t)) = |e_{vi}(t)| - \varsigma_{v2}$ and $f_i(t, \boldsymbol{e}_{\varphi i}(t)) = \|\boldsymbol{e}_{\varphi i}(t)\| - \varsigma_{\varphi2}$. Choose $\varsigma_{v2} = 0.5$ and $\varsigma_{\varphi2} = 0.2$.

The numbers of information transmission under different communication mechanisms are given in Table II. While taking the tracking maneuver of UAV 3 for example, the comprehensive performances under SECM and DECM are plotted in Fig. 7. From Table II, one can see that compared with PCM and SECM, DECM leads to least transmitted information, thus reducing the occupancy of limited communication resources. Even though
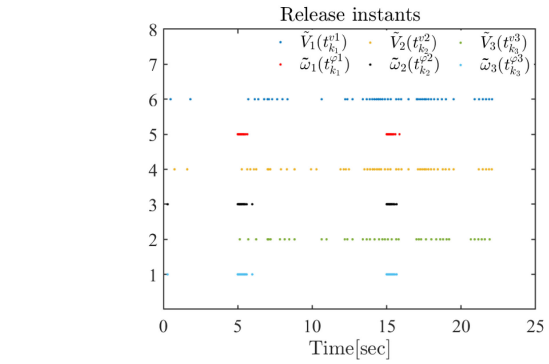
with least communication transmission, the desired coordinated tracking under DECM can be still accomplished with scheduled precise requirements. This point is clearly shown in Fig. 7, where the responses of velocities and attitudes for DECM are almost similar to SECM. As a result, it can be concluded that the proposed dynamic event-based control scheme provides a better balance between saving communication resources and achieving well tracking performances than PCM and SECM.

Case 3: To further evaluate the sensitivity of proposed event-triggered conditions, we consider the following four different fault modes:

Fault mode 1: As defined in above simulation scenario, the thrust of UAV 3 suffers the loss of effectiveness, that is, $\rho_{T_3} = 0.9$ during $t \in (2, 5]$s.

Fault mode 2: Based on the fault mode 1, the period of time when the thrust loses its effectiveness is enlarged, that is, $\rho_{T_3} = 0.9$ during $t \in (2, 8]$s.

Fault mode 3: The aileron of UAV 3 loses its effectiveness described by $\boldsymbol{\rho}_{\delta_3} = \text{diag}\{0.9, 1, 1\}$ during $t \in (5, 10]$s.

Fault mode 4: The rudder of UAV 3 loses its effectiveness described by $\boldsymbol{\rho}_{\delta_3} = \text{diag}\{1, 1, 0.9\}$ during $t \in (5, 10]$s.

Based on above fault modes, the fault-tolerant performances of UAV 3 for different fault modes are shown in Fig. 8. Robustness with proposed controller is demonstrated in case of above four fault modes as presented in Fig. 8. The data release

TABLE II
THE NUMBER OF DATA TRANSMISSION FOR EACH UAV UNDER DIFFERENT COMMUNICATION MECHANISMS

Transmitted data	$\tilde{V}_1\left(t_{k_1}^{v1}\right)$	$\tilde{\omega}_1\left(t_{k_1}^{\varphi1}\right)$	$\tilde{V}_2\left(t_{k_2}^{v2}\right)$	$\tilde{\omega}_2\left(t_{k_2}^{\varphi2}\right)$	$\tilde{V}_3\left(t_{k_3}^{v3}\right)$	$\tilde{\omega}_3\left(t_{k_3}^{\varphi3}\right)$
PCM	2500	2500	2500	2500	2500	2500
SECM	187	583	148	582	146	584
DECM	51	143	52	149	42	146
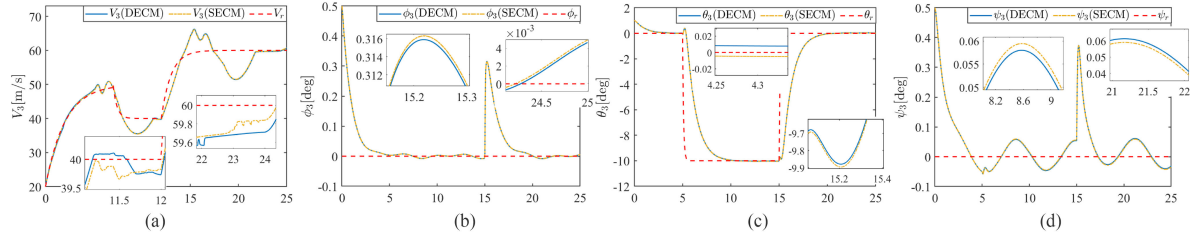
Fig. 7. Velocity and attitude tracking of UAV 3 under DECM and SECM. (a)–(d) show the curves of state responses. (a) Velocity response (b) Roll angle response (c) Pitch angle response (d) Yaw angle response.
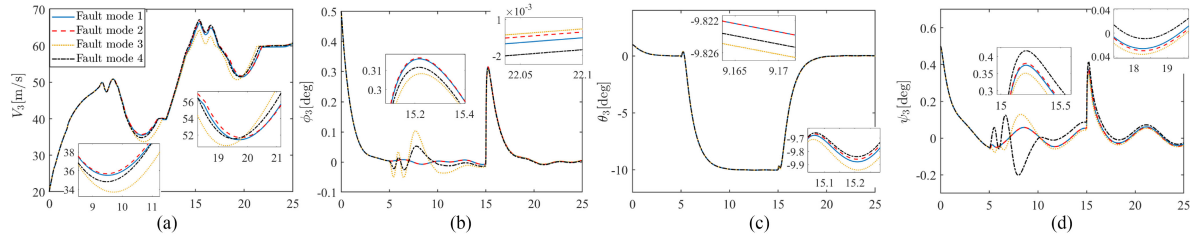

Fig. 8. Velocity and attitude tracking of UAV 3 under different fault modes. (a)–(d) show the curves of state responses. (a) Velocity response (b) Roll angle response (c) Pitch angle response (d) Yaw angle response.
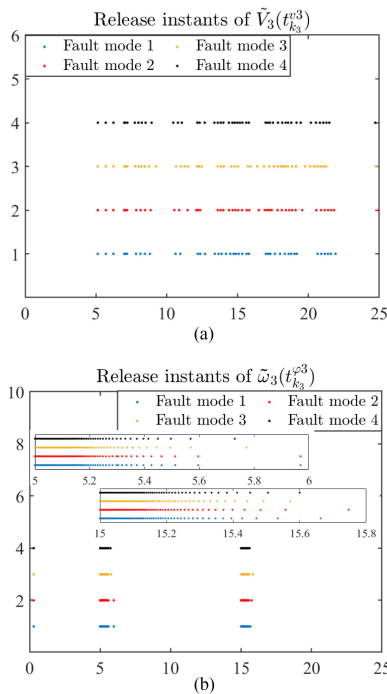

Fig. 9. Release instants of velocity and attitude data of UAV 3 under different fault modes.

TABLE III
THE NUMBER OF DATA TRANSMISSION UNDER DIFFERENT FAULT MODES

Transmitted data	$\tilde{V}_3\left(t_{k_3}^{v3}\right)$	$\tilde{\omega}_3\left(t_{k_3}^{\varphi3}\right)$
Fault mode 1	42	146
Fault mode 2	45	147
Fault mode 3	46	146
Fault mode 4	47	145

instants of velocity and attitude for UAV 3 with different faults are presented in Fig. 9. Besides, the corresponding amount of exchange of information under four fault modes are given in Table III. From Fig. 8, Fig. 9 and Table III, we can notice that the fault-tolerant property guarantees the stable tracking of UAV 3 in the presence of four different fault modes, and thus no additional communications are triggered in such cases.

V. CONCLUSION

This work investigates the event-based fault-tolerant coordinated control problem of multiple fixed-wing UAVs. A novel event-triggered communication mechanism has been presented, wherein the threshold parameter is not fixed permanently but determined by a dynamic rule. By imposing proposed event-triggered mechanisms on translational and rotational subsystems

respectively, the inter-agent communication has been regulated to avoid the unnecessary communications and save on network resources. Furthermore, an event-based coordinated control scheme has been designed using only locally triggered state information at discretized instants. This work lays down the groundwork for other coordinated control problems of UAVs including formulating and maintaining a particular formation shape. Additionally, note that the extension of event-triggered mechanism to sensor-to-controller channel for UAV system remains open and deserves further investigation.

REFERENCES

[1] T. Kim and D. Qiao, "Energy-efficient data collection for IoT networks via cooperative multi-hop UAV networks," *IEEE Trans. Veh. Technol.*, vol. 69, no. 11, pp. 13796–13811, Nov. 2020.

[2] H. Qiu and H. Duan, "Multiple UAV distributed close formation control based on in-flight leadership hierarchies of pigeon flocks," *Aerosp. Sci. Technol.*, vol. 70, pp. 471–486, 2017.

[3] Y. Chen, D. Chang, and C. Zhang, "Autonomous tracking using a swarm of UAVs: A constrained multi-agent reinforcement learning approach," *IEEE Trans. Veh. Technol.*, vol. 69, no. 11, pp. 13702–13717, Nov. 2020.

[4] Y. Wang, M. Shan, and D. Wang, "Motion capability analysis for multiple fixed-wing UAV formations with speed and heading rate constraints," *IEEE Trans. Control Netw. Syst.*, vol. 7, no. 2, pp. 977–989, Jun. 2020.

[5] Z. Yu *et al.*, "Fractional-order adaptive fault-tolerant synchronization tracking control of networked fixed-wing UAVs against actuator-sensor faults via intelligent learning mechanism," *IEEE Trans. Neural Netw. Learn. Syst.*, vol. 32, no. 12, pp. 5539–5553, Dec. 2021, doi: 10.1109/TNNLS.2021.3059933.

[6] M. Lv, W. Yu, J. Cao, and S. Baldi, "Consensus in high-power multi-agent systems with mixed unknown control directions via hybrid Nussbaum-based control," *IEEE Trans. Cybern.*, to be published, doi: 10.1109/TCYB.2020.3028171.

[7] M. Lv, B. De Schutter, C. Shi, and S. Baldi, "Logic-based distributed switching control for agents in power chained form with multiple unknown control directions," *Automatica*, vol. 137, Mar. 2022, Art. no. 110143.

[8] Z. Yu, Y. Zhang, Z. Liu, Y. Qu, and C. Y. Su, "Distributed adaptive fractional-order fault tolerant cooperative control of networked unmanned aerial vehicles via fuzzy neural networks," *IET Control Theory Appl.*, vol. 13, no. 17, pp. 2917–2929, 2019.

[9] Z. Yu, Y. Qu, and Y. Zhang, "Distributed fault-tolerant cooperative control for multi-UAVs under actuator fault and input saturation," *IEEE Trans. Control Syst. Technol.*, vol. 27, no. 6, pp. 2417–2429, Nov. 2019.

[10] Y. Wang, T. Zhang, Z. Cai, J. Zhao, and K. Wu, "Multi-UAV coordination control by chaotic grey wolf optimization based distributed MPC with event-triggered strategy," *Chin. J. Aeronaut.*, vol. 33, no. 11, pp. 2877–2897, Nov. 2020. [Online]. Available: https://doi.org/10.1016/j.cja.2020.04.028

[11] T. Z. Muslimov and R. A. Munasypov, "Adaptive decentralized flocking control of multi-UAV circular formations based on vector fields and backstepping," *ISA Trans.*, vol. 107, pp. 143–159, Dec. 2020. [Online]. Available: https://doi.org/10.1016/j.isatra.2020.08.011

[12] K. Guo, X. Li, and L. Xie, "Ultra-wideband and odometry-based cooperative relative localization with application to multi-UAV formation control," *IEEE Trans. Cybern.*, vol. 50, no. 6, pp. 2590–2603, Jun. 2020.

[13] J. Zhang, J. Yan, and P. Zhang, "Multi-UAV formation control based on a novel back-stepping approach," *IEEE Trans. Veh. Technol.*, vol. 69, no. 3, pp. 2437–2448, Mar. 2020.

[14] X. Dong, Y. Hua, Y. Zhou, Z. Ren, and Y. Zhong, "Theory and experiment on formation-containment control of multiple multirotor unmanned aerial vehicle systems," *IEEE Trans. Automat. Sci. Eng.*, vol. 16, no. 1, pp. 229–240, Jan. 2019.

[15] G. S. Seyboth, D. V. Dimarogonas, and K. H. Hohansson, "Event-based broadcasting for multi-agent average consensus," *Automatica*, vol. 49, no. 1, pp. 245–252, 2013.

[16] X. Yi, T. Yang, J. Wu, and K. H. Johansson, "Distributed event-triggered control for global consensus of multi-agent systems with input saturation," *Automatica*, vol. 100, pp. 1–9, 2019.

[17] P. Duan, K. Liu, N. Huang, and Z. Duan, "Event-based distributed tracking control for second-order multiagent systems with switching networks," *IEEE Trans. Syst., Man, Cybern. Syst.*, vol. 50, no. 9, pp. 3220–3230, Sep. 2020.

[18] Y. Qian, L. Liu, and G. Feng, "Output consensus of heterogeneous linear multi-agent systems with adaptive event-triggered control," *IEEE Trans. Automat. Control*, vol. 64, no. 6, pp. 2606–2613, Jun. 2019.

[19] C. Peng, J. Zhang, and Q. Han, "Consensus of multiagent systems with nonlinear dynamics using an integrated sampled-data-based event-triggered communication scheme," *IEEE Trans. Syst., Man, Cybern. Syst.*, vol. 49, no. 3, pp. 589–599, Mar. 2019.

[20] C. Wang, C. Wen, L. Guo, and L. Xing, "Adaptive consensus control for nonlinear multiagent systems with unknown control directions using event-triggered communication," *IEEE Trans. Cybern.*, to be published, doi: 10.1109/TCYB.2020.3022423.

[21] X. Ge and Q. L. Han, "Distributed formation control of networked multi-agent systems using a dynamic event-triggered communication mechanism," *IEEE Trans. Ind. Electron.*, vol. 64, no. 10, pp. 8118–8127, Oct. 2017.

[22] E. Garcia, Y. Cao, and D. W. Casbeer, "Decentralized event-triggered consensus with general linear dynamics," *Automatica*, vol. 50, no. 10, pp. 2633–2640, 2014.

[23] C. Viel, S. Bertrand, S. Kieffer, and H. Piet-Lahanier, "Distributed event-triggered control strategies for multi-agent formation stabilization and tracking," *Automatica*, vol. 106, pp. 110–116, 2019.

[24] A. Girard, "Dynamic triggering mechanisms for event-triggered control," *IEEE Trans. Autom. Control*, vol. 60, no. 7, pp. 1992–1997, Jul. 2015.

[25] V. S. Dolk, D. P. Borgers, and W. P. M. Heemels, "Dynamic event-triggered control: Tradeoffs between transmission intervals and performance," *Proc. IEEE Conf. Decis. Control*, 2014, pp. 2764–2769.

[26] Z. Yu, Z. Liu, Y. Zhang, Y. Qu, and C. Y. Su, "Distributed finite-time fault-tolerant containment control for multiple unmanned aerial vehicles," *IEEE Trans. Neural Netw. Learn. Syst.*, vol. 31, no. 6, pp. 2077–2091, Jun. 2020.

[27] A. Abbaspour, K. K. Yen, P. Forouzannezhad, and A. Sargolzaei, "A neural adaptive approach for active fault-tolerant control design in UAV," *IEEE Trans. Syst., Man, Cybern. Syst.*, vol. 50, no. 9, pp. 3401–3411, Sep. 2020.

[28] B. Zhang, X. Sun, S. Liu, M. Lv, and X. Deng, "Event-triggered adaptive fault-tolerant synchronization tracking control for multiple 6-DOF fixed-wing UAVs," *IEEE Trans. Veh. Technol.*, vol. 71, no. 1, pp. 148–161, Jan. 2022.

[29] H. Castaneda, O. S. Salas-Pena, and J. Le n-Morales, "Extended observer based on adaptive second order sliding mode control for a fixed-wing UAV," *ISA Trans.*, vol. 66, pp. 226–232, 2017.

[30] E. Oland, "Nonlinear control of fixed-wing unmanned aerial vehicles," Ph.D. dissertation, Norwegian Univ. Sci. Technol., Fac. Inf. Technol., Math. Elect. Eng., Dept. Eng. Cybern., Trondheim, Norway, 2014.

[31] M. Lv, W. Yu, J. Cao, and S. Baldi, "A separation-based methodology to consensus tracking of switched high-order nonlinear multi-agent systems," *IEEE Trans. Neural Netw. Learn. Syst.*, 2021, to be published, doi: 10.1109/TNNLS.2021.3070824.

[32] W. Ren, "On consensus algorithms for double-integrator dynamics," *IEEE Trans. Automat. Control*, vol. 53, no. 6, pp. 1503–1509, Jul. 2008.

[33] W. E. Dixon, "Adaptive regulation of amplitude limited robot manipulators with uncertain kinematics and dynamics," *IEEE Trans. Automat. Control*, vol. 52, no. 3, pp. 488–493, Mar. 2007.

[34] S. Zeghlache, H. Mekki, A. Bougueera, and A. Djerioui, "Actuator fault tolerant control using adaptive RBFNN fuzzy sliding mode controller for coaxial octorotor UAV," *ISA Trans.*, vol. 8, pp. 267–278, 2018.

[35] F. Jiang, F. Pourpanah, and Q. Hao, "Design, implementation, and evaluation of a neural-network-based quadcopter UAV system," *IEEE Trans. Ind. Electron.*, vol. 67, no. 3, pp. 2076–2085, Mar. 2020.

[36] T. Dierks and S. Jagannathan, "Output feedback control of a quadrotor UAV using neural networks," *IEEE Trans. Neural Netw.*, vol. 21, no. 1, pp. 50–66, Jan. 2010.

[37] Y. Song, L. He, D. Zhang, J. Qian, and J. Fu, "Neuroadaptive fault-tolerant control of quadrotor UAVs: A more affordable solution," *IEEE Trans. Neural Netw. Learn. Syst.*, vol. 30, no. 7, pp. 1975–1983, Jul. 2019.